Research Article Vol. 30, No. 1 / 3 Jan 2022 / Optics Express 676
Optics EXPRESS

Rapid fabrication of sub-micron scale functional optical microstructures on the optical fiber end faces by DMD-based lithography

LUMING WANG,[1,2] NINGNING LUO,[1,2,3] ZHIMIN ZHANG,[1,2] HAIFENG XIAO,[1,2] LONG MA,[1,2] QINGWANG MENG,[1,2] AND JIULIN SHI[1,2,4]

[1] *Key Laboratory of Opto-Electronic Information Science and Technology of Jiangxi Province, Nanchang Hangkong University, Nanchang, China*
[2] *Key Laboratory of Nondestructive Test (Ministry of Education), Nanchang Hangkong University, Nanchang, China*
[3] *ningningluo2002@126.com*
[4] *jiulinshi@126.com*

Abstract: The rapid development of optical fiber application systems puts forward higher requirements for the miniaturization and integration of optical fiber devices. One promising solution is to integrate diffractive optical microstructures on the end faces of optical fibers. However, rapid microfabrication on such tiny and irregular substrates is a challenge. In recent years, Femtosecond laser polymerization technology has become an effective solution to the challenge, which can be flexibly applied for the fabrication of complex 3D microstructures with ultra-high resolution. When the demand for the lithography resolution is not very high, other microfabrication methods with a lower technical threshold may be developed for achieving a balance between fabrication precision, cost and efficiency. In this paper, we report a Digital Micromirror Device (DMD) based lithography method dedicated to the fabrication of functional optical microstructures on the optical fiber end faces. Especially, it's also applicable to single-mode fibers (SMFs). By the projection via a 40x objective lens, the fabrication resolution of 0.405 μm was achieved within an exposure area of 209.92 μm × 157.44 μm. We evaluated the microfabrication results by the photomicrographs and the optical diffraction modulation effects of the functional optical microstructures. This method provides a new idea for fabricating both hybrid optical fiber devices and SMF devices, and it may be an alternative method for resolving the conflict between the precision, the cost and the efficiency.

1. Introduction

Powered by the trend of deeper integration of optical-fiber-based systems, functional optical microstructures directly fabricated on the optical fiber end faces are gaining attention and popularity. With regard to optical fiber communication systems, beam splitting can usually be achieved by diffractive optical elements fabricated on fiber facet [1], the concentric grating on fiber facet plays a supporting role in orbital angular momentum generation [2–3], and the microlens and microlens array on fiber facet can be used as a promising fiber endoscope [4] and can significantly enhance the coupling efficiency between fibers [5–6]. Furthermore, the fork-shaped grating on the fiber facet can generate a vortex light beam [7] to help improve the channel capacity of communication systems. Fresnel plates and wedge-like structures on fiber facet can participate in the formation of the optical potential-well, on which the fiber optical tweezers rely [8–11]. Various other microstructures have also been used in diverse fiber probes [12–16]. At the forefront of the field of fiber-tip microstructures, S. Schmidt *et al.* [17] achieved a novel method to design fiber-tip freeform holograms and modulate the fiber output as self-defined complex illumination patterns.

#445677 https://doi.org/10.1364/OE.445677
Journal © 2022 Received 12 Oct 2021; revised 6 Dec 2021; accepted 13 Dec 2021; published 24 Dec 2021

Optics EXPRESS

Compared with conventional fiber optic devices, these functional optical microstructures directly fabricated on fiber facet have remarkable advantages of smaller volume and better performance. They are generally used as core components in various optical-fiber-based systems. Therefore, convenient, low-cost, and high-efficiency microfabrication methods for the microstructures on fiber facet are being widely explored.

Most of the existing microfabrication approaches have the disadvantage of high cost. For example, mask-based lithography [18] and nano-imprint lithography [19–21] enable batch fabrication, but the use of physical masks causes an increase in the production cost, in addition, they are particularly unsuitable for the small area substrate such as fiber end faces. Electron beam lithography [22–24], focused ion beam milling [2,10,25,26], and direct laser writing [27–30] can realize nanometer-scale precision fabrication. Particularly in 2010, Malinauskas *et al.* [31] have achieved the fabrication of hybrid and integrated micro-optical elements on the fiber end faces by femtosecond laser polymerization. During these years, more complex optical fiber-tip microstructures have been fabricated and well applied [32,33], and a photoresist with high laser damage threshold suitable for multi-photon polymerization was developed by Kabouraki *et al.* [34]. But the above methods may be costly and overqualified for the fabrication of C-band optical fiber devices commonly with micrometer-scale feature sizes, especially binary microstructures.

As a promising technology, Digital Micromirror Device (DMD) based maskless lithography which is characterized by the outstanding advantages of low cost and high efficiency, has attracted a great deal of attention in the field of rapid fabrication of micron-scale microstructures [35–38]. Through electronically controlling the hundreds of thousands of micromirrors on the DMD chip to rotate to the "ON" state or the "OFF" state, gray-scale images can be conveniently converted to photoresist microstructures upon the ultraviolet (UV) light irradiation. Furthermore, various resolution enhancement techniques such as proximity optimization [39], wobulation technique [40–41], and multiple patterning with process optimization method [42] have pushed the improvement of lithography quality. So the DMD-based maskless lithography has been implemented to fabricate functional microstructures on the optical fiber facet in recent years.

Kim *et al*. have reported a method for fabricating optical microstructures on the end faces of an optical fiber by DMD-based lithography, providing a spatial resolution of 2.2 μm [35]. They performed that method on a specific facet of specially customized hybrid optical fiber comprising a single-mode fiber (SMF) serially fusion-spliced with a coreless fiber (CLF) segment. The core diameter of an SMF is around 9 μm, thus with Kim's method, it's difficult to form effective functional optical microstructures on the fiber core of an SMF. Therefore, for the fabrication of optical microstructures on the fiber core of an SMF, it's a great challenge to find out a balance between fabrication precision, cost, and efficiency.

In order to cope with the challenge posed by the conflict of fabrication precision, cost, and efficiency, in this study, a convenient fabrication method based on DMD maskless lithography and additional processes is proposed especially for fabricating optical microstructures on the fiber end face. This method can be used to rapidly fabricate optical microstructures on the end face of optical fiber or the fiber jumper with a minimum feature size of 0.405 μm. Besides, a direct photoresist spin-coating process is proposed, by which the photoresist can be coated directly on the fiber facets, thus enhancing the fabrication efficiency and adaptability. To verify the feasibility of the proposed method and the experimental results, a laser beam was coupled into the SMF, so that the optical diffraction modulation results of the functional optical microstructures fabricated on the SMF end face can be intuitively observed.

2. Experimental setup and fabrication on the quartz glass substrates

A schematic diagram and a photograph of the DMD-based experimental system for the fabrication of functional optical microstructures are shown in Fig. 1 and Fig. 2 respectively.

Optics EXPRESS

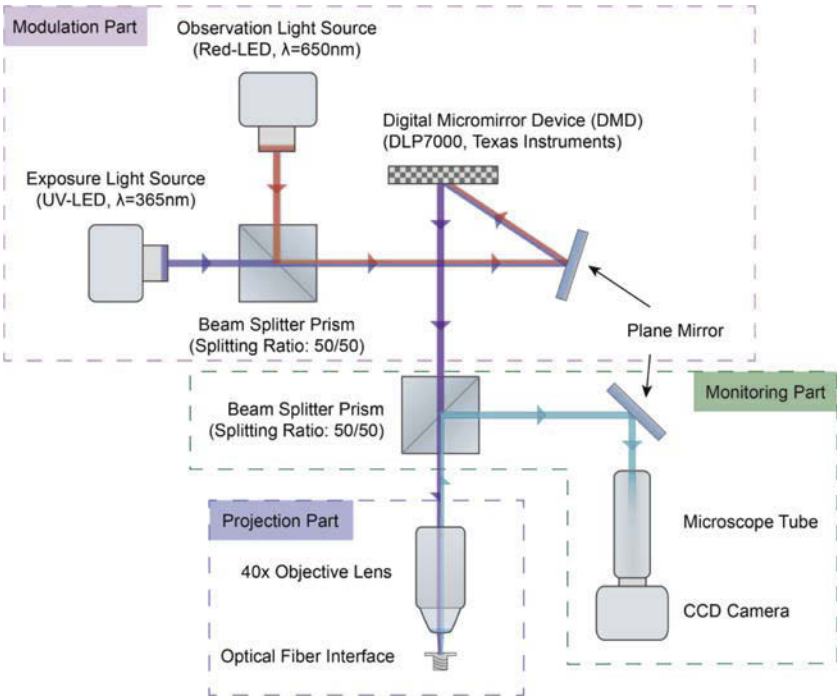

Fig. 1. Schematic diagram of the DMD-based experimental system for the fabrication of functional optical microstructures.

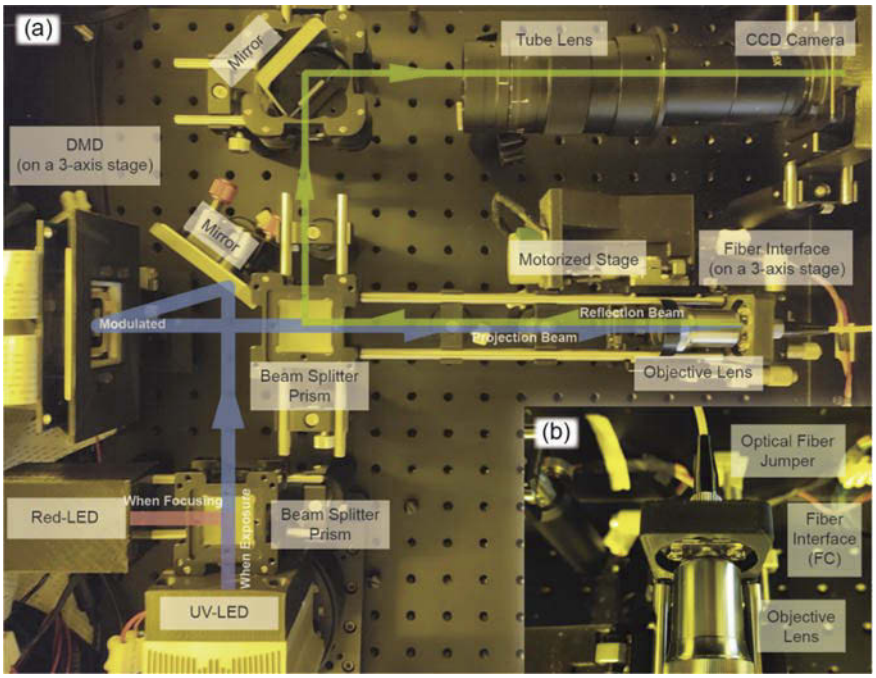

Fig. 2. (a) Photograph of the DMD-based experimental system. (b) Enlarged photograph of the projection part in the right part of (a).

Optics EXPRESS

As shown in Fig. 1, the experimental system is composed of modulation, projection, and monitoring parts. In the modulation part, a Texas Instruments DMD (DLP7000) with an array of 1024×768 micromirrors with 13.68 μm wide acts as a reflective spatial light modulator, covering an area of 14.008 mm × 10.506 mm. A UV light-emitting diode (LED) with a center wavelength of 365 nm is used as the exposure light source. The UV light beam is transmitted through a beam splitter prism (50/50 splitting ratio), reflected from a plane mirror, and then incident on DMD at a spatial angle of 24°. Subsequently, the light field will be modulated by the pre-loaded grayscale pattern on DMD. In the Projection part, the UV light field modulated by DMD is projected onto the photoresist-coated fiber end face through a 40x objective lens (NA = 0.65, working distance = 0.632 mm, focal length = 4.65 mm). The optical fiber or the fiber jumper is fixed into the optical path via a Ferrule Connector interface (FC, alternatively other standard optical fiber interfaces) installed on a motorized stage. Thus the distance between the objective lens and the fiber end face can be precisely adjusted by the motorized stage.

When the photoresist-coated fiber is placed at the working plane of the objective lens, theoretically, the exposure area is about 266.24 μm 199.68 μm in a single process. So the SMF fiber core with a diameter of 9 μm can be covered completely in a single exposure. In the Monitoring part, a red LED with a center wavelength of 650 nm acts as an observation light source. The observation light beam and the exposure light beam are combined by the beam splitter prism as mentioned earlier. By another beam splitter prism with a 50/50 splitting ratio, the observation light field reflected from the fiber end face will be reflected again, and finally captured by a CCD camera. Thus, the focusing process can be precisely manipulated under the monitor by a CCD camera.

Prior to the final fabrication on fiber end faces, it is necessary to perform a verification experiment on conventional substrates such as quartz glass substrates. A positive-tone photoresist KMP-C7500 (Kempur Microelectronics Inc.) is spin-coated at 2000 rpm onto a clean quartz glass substrate for at least 40 s, and then soft-baked at 90 °C for 60 s. A photoresist thin film with a thickness of about 1.3 μm can be obtained. For fiber-tip diffraction optical devices, the photoresist transmission at different wavelengths is important to evaluate whether such devices can work as expected in a specific band. We obtain the transmission curve from the photoresist manufacturer as shown in Fig. 3(a), which shows that the photoresist we used has high transmission in the visible light band. So we can easily evaluate the performance of fiber-tip devices by coupling a visible light into an optical fiber. Bleaching is a photochemical reaction that occurs during the exposure process. Hence, in Fig. 3(a), we can regard "bleached" as exposed and "unbleached" as unexposed. Figure 3(b) shows the spin-coating curve of the photoresist. We can obtain the expected thickness by controlling the spin speed. In this part of the experiments on glass slide substrates, we fix the photoresist-coated substrate in the holder of the experimental system, which is in the same position as the optical fiber interface.

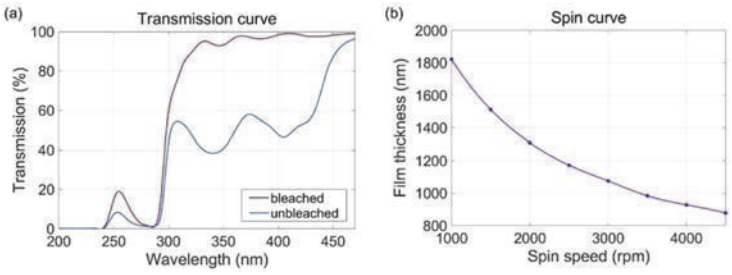

Fig. 3. (a) Transmission curve of the positive-tone photoresist of KMP-C7500 (Kempur Microelectronics Inc.). (b) Spin-coating curve of the photoresist.

Optics EXPRESS

Figures 4(a)-4(d) show some examples of mask patterns displayed on DMD, such as linear gratings and Dammann gratings. The minimum feature sizes in Figs. 4(b) and 4(d) are both two DMD mirror-pixels. In Figs. 4(c) and 4(d), the regions surrounded by the orange solid lines indicate one period of the Dammann grating.

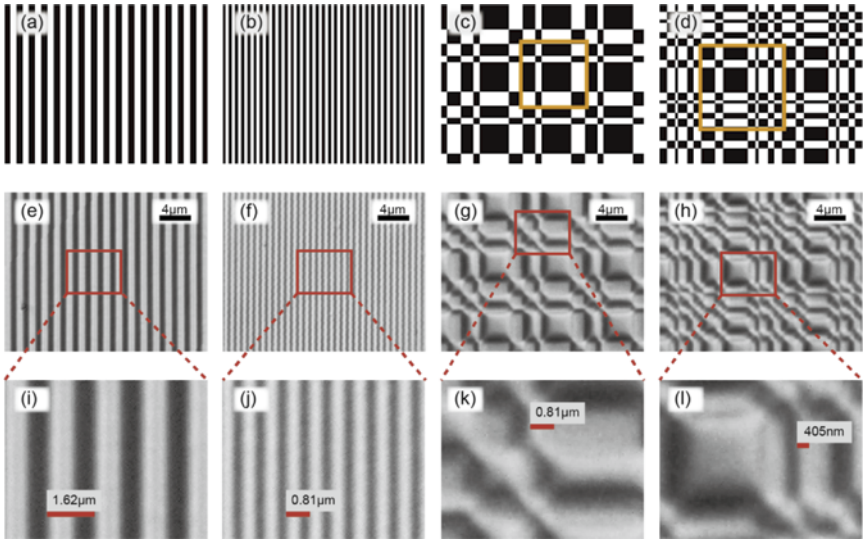

Fig. 4. The experimental results that using DMD-based lithography on quartz glasses. (a-d) Gray-scale mask patterns projected onto DMD chip, (e-h) Photomicrographs of microstructures observed under a microscope, (i-l) Enlarged views of the regions surrounded by the red solid lines in (e)-(h).

For different microstructures with different feature sizes, the exposure time for these mask patterns ranges from 1 s to 5 s. The i-line UV dose on the substrate should be ranged from about 15 to 75 mJ/cm^2. After development in 4‰ NaOH solution for 4 s, the formed microstructures are measured by a microscope (BX46, Olympus Corporation). Figures 4(e) and 4(f) show the fabricated linear gratings with periods of 1.62 μm and 0.81 μm, the duty cycles of which are both 50%. Figure 4(g) shows a fabricated 7×7 Dammann grating with the minimum feature size of 0.81 μm and Fig. 4(h) shows a 15×15 Dammann grating with the minimum feature size of 0.405 μm. The experimental result shows that the DMD based lithography system we proposed is capable of fabricating photoresist microstructures with a precision of approximately 0.4 μm within an exposure area of 209.92 μm 157.44 μm. The actual demagnification factor of the objective lens is approximately 67.

3. Fabrication of functional optical microstructures on the SMF end faces

The fabrication process of functional optical microstructures on the SMF end faces is described in Fig. 5. First, the fiber end face should be cleaned carefully as shown in Fig. 5(a). Then the photoresist is uniformly coated on the end face of an optical fiber ferrule with a diameter of about 2.5 mm. The spin-coating process is illustrated in Figs. 5(c)–5(d). Because the following soft-baking process will make it difficult to remove the residual photoresist on the side of optical fiber ferrule, so it should be promptly cleaned with alcohol. Next, as shown in Fig. 5(e), the photoresist-coated fiber end face is soft-baked in a convection oven at 100 °C for 60 s and then cooled down to room temperature naturally. Following the above treatments, the fiber jumper is locked onto the optical fiber interface of the experimental system. Under the observation light source illumination, we precisely adjust the position of the fiber end face so that the digital mask

Optics EXPRESS

displayed on the DMD can be projected on the photoresist layer on the fiber end face. The whole adjustment process can be monitored by the monitoring part in our experimental system. After compensating the optical path difference which is introduced by switching the light source from the red LED to the UV LED, the exposure process is operated under UV illumination as shown in Fig. 5(f). The exposure time is the same as that used in the microfabrication on quartz glass substrates. Finally, in the development process, as shown in Fig. 5(g), the exposed optical fiber is immersed in a 4‰ NaOH solution for 4 s. After finishing all the steps above, the microstructures are finally fabricated on the optical fiber end faces, as shown in Fig. 5(h).

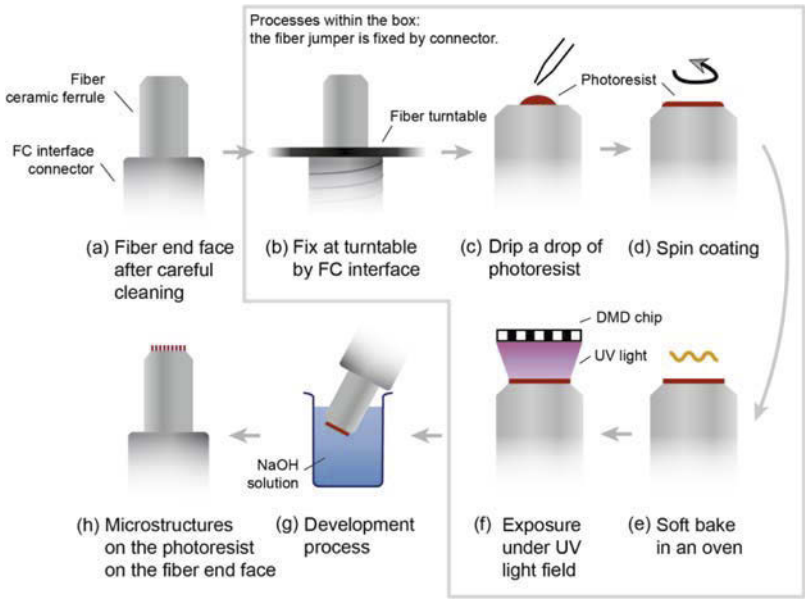

Fig. 5. Schematic overview of the fabrication process of microstructures on fiber end faces. (a) Cleaning the fiber end face carefully, usually with a concentrated NaOH solution. (b) Fixing the fiber end to the turntable by FC interface. (c) Dripping the photoresist over the entire fiber end face. (d) Spin coating for forming a photoresist film with a thickness of about 1.3 μm. (e) Soft baking in a convection oven at 100 °C for 60 s. (f) Locking the fiber jumper onto the optical fiber interface of the experimental system and exposing it under the UV light. (g) Developing in a 4‰ NaOH solution for 4 s and then cleaning with deionized water. (h) Photoresist microstructures formed on the fiber end face.

Unlike the spin-coating process on the quartz glasses, a specialized device for directly spin coating photoresist on fiber end-faces has been designed as shown in Fig. 6. The upper part is a concentric turntable, and the fiber jumper interfaces are symmetrically placed around the rotation axis of the turntable. After being locked by the fiber FC interfaces, the fiber end faces will be held horizontally during the spin-coating process, which aims to obtain a smooth photoresist surface on the fiber end face. The actual rotational speed of the turntable will be affected by the centrifugal force of the rotating fiber jumper, therefore, the rotational speed negative feedback is introduced to ensure that the actual rotational speed of the turntable is as close to the set speed as possible.

It is worth mentioning that the control part is designed to provide three gears speed in a single spin-coating process. Apart from the low speed for spreading the photoresist and the medium speed for maintaining the photoresist thickness, a high acceleration is needed at the end of the spin-coating process to remove the excess photoresist on the edge of the fiber ferrule. The spin-coating process in our experiment is performed at 2000 rpm (the medium speed) for 45 s and

Optics EXPRESS

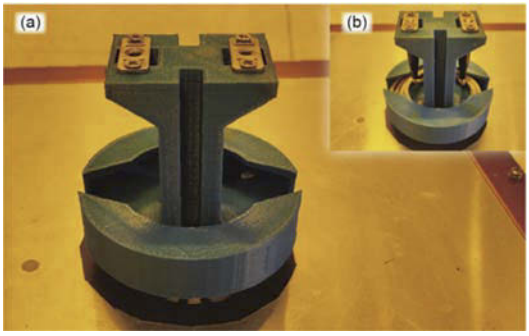

Fig. 6. (a) Photograph of the apparatus for directly spin coating photoresist on the fiber end faces. (b) Photograph of the optical fibers being locked in the turntable.

5000 rpm (the extra high acceleration speed) for 2 s in the end. Besides, a vibration-absorbing structure is designed onto the rotation shaft to reduce the thickness inhomogeneity of the photoresist film caused by the vibration.

Diverse functional optical microstructures are finally fabricated on the SMF end faces by using the DMD-based experimental system we proposed. Figure 7 shows the optical microscope images for linear gratings and circular Dammann grating. The linear grating with the minimum feature size of 0.405 μm has been successfully fabricated on the SMF end face.

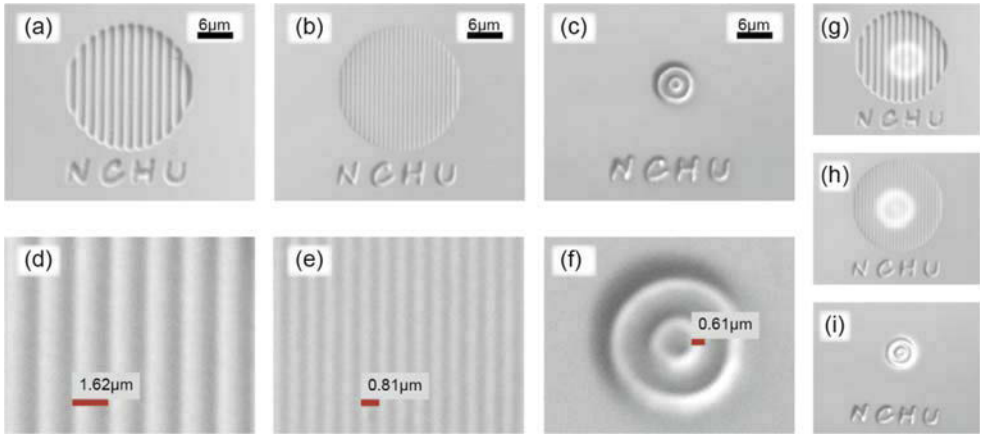

Fig. 7. The fabrication results using DMD-based lithography on the fiber end faces. Both letters and microstructures outside the optical fiber core are used only for evaluation. "NCHU" is the abbreviation for "Nanchang Hangkong University". (a) A linear grating with a period of 1.62 μm and a duty cycle of 50%. (b) A linear grating with a period of 0.81 μm and a duty cycle of 50%. (c) A circular Dammann grating with a minimum feature size of 0.61 μm. (d-f) The enlarged images of (a)-(c). (g-i) A white light beam is coupled into the optical fiber from another facet to indicate the position relationship between the optical fiber core and the microstructure.

To further evaluate the lithography quality, an optical profilometer (white light interference, KLA-Tencor MicroXAM-100) is used to measure the fabricated profile. Figure 8 shows the 3D profile of a linear grating with a period of 1.62 μm on the fiber end face.

The desired profile is a binary grating that has only two steps. But due to some factors such as the modulation property of DMD, the responding property of photoresist and the exposure, development process, the actual grating has a sinusoidal profile. In Fig. 8(b), we select partial

Optics EXPRESS

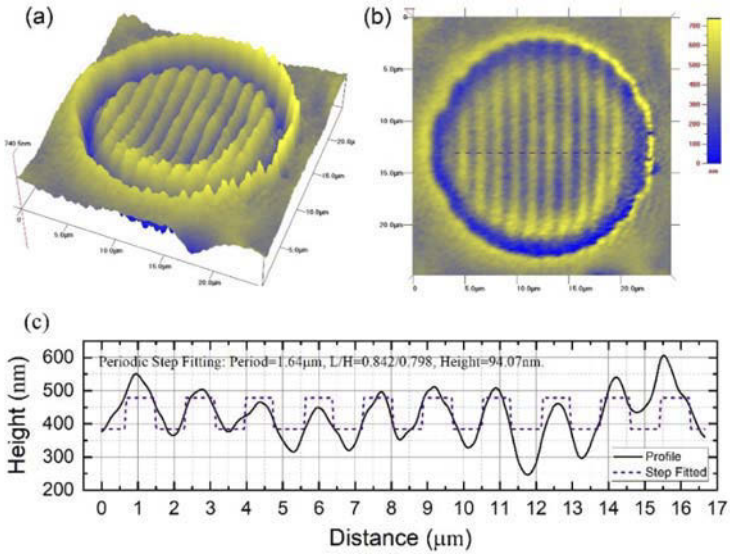

Fig. 8. The end face profile of the linear grating with a period of 1.62 μm, measured by an optical profilometer. (a) 3D profile of the linear gating, (b) Top view of the linear grating, (c) Cross-sectional view measured along the dotted line in (b). (a) and (b) share the same color bar in the upper right corner.

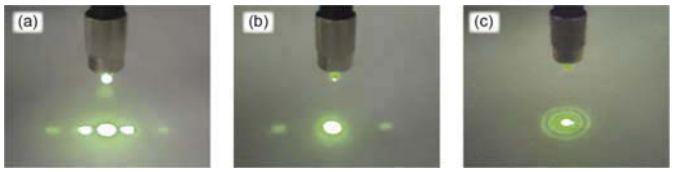

Fig. 9. Optical diffraction modulation effects of the functional optical microstructures fabricated on the SMF end faces. (a) A linear grating with a period of 1.62 μm and a duty cycle of 50%. (b) A linear grating with a period of 0.81 μm and a duty cycle of 50%. (c) A circular Dammann grating with a minimum feature size of 0.61 μm.

grating structures along the horizontal direction and draw a cross-sectional view (as shown in Fig. 8(c)) along the dotted line. Then we fit a periodic step function for the cross-sectional profile. So we can obtain some grating parameters as labeled in the upper of Fig. 8(c). From the above parameters obtained from the fitted step function, both the grating period (1.64μm) and the duty cycle (about 48.6%) are highly consistent with our expectations (the period is 1.62 μm and the duty cycle is 50%).

4. Discussions

To further verify the validity of the DMD-based lithography we proposed, we demonstrate the optical diffraction modulation effects of the functional optical microstructures fabricated on the optical fiber end faces. A green laser beam at 532 nm is coupled into the optical fiber from another side and emitted from the optical fiber end face on which the microstructures are fabricated. The optical diffraction modulation effects can be observed as shown in Fig. 9. These fiber jumpers are fixed at about 2 cm height above the white paper.

Optics EXPRESS

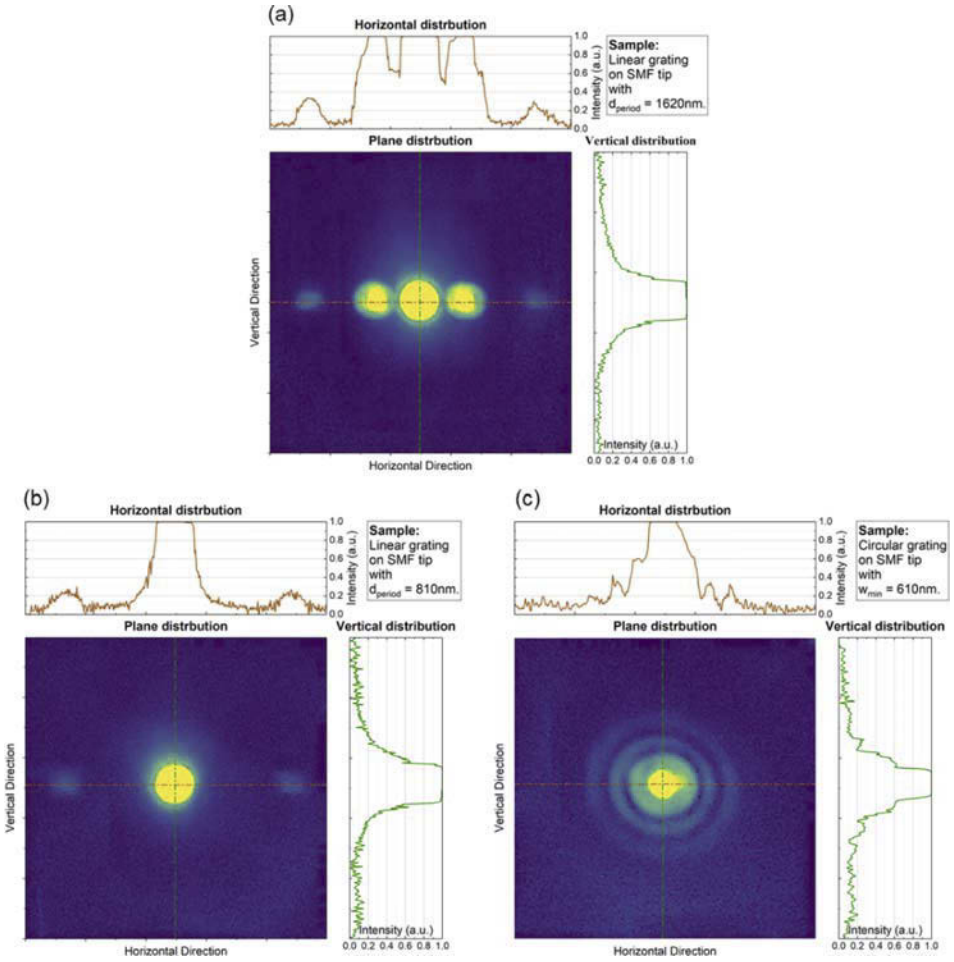

Fig. 10. The X/Y cross-sectional view of the diffraction patterns corresponding to Fig. 9. The intensity may be saturated due to the performance of CCD camera. (a) A linear grating with a period of 1.62 μm and a duty cycle of 50%. (b) A linear grating with a period of 0.81 μm and a duty cycle of 50%. (c) A circular Dammann grating with a minimum feature size of 0.61 μm.

We conduct quantitative analysis of the diffraction patterns modulated by the fiber-tip microstructures in Fig. 7. Figure 10 shows the X/Y cross-sectional view of the diffraction patterns respectively.

Then we further demonstrate the theoretical simulations to evaluate the diffraction pattern. First, we take the Fourier transform of the screen function which is obtained by longitudinally extended the fabricated profile in Fig. 8(c). The cross-sectional view of the theoretical diffraction pattern is shown in Fig. 11, from which we can obtain that the intensity ratio of the "tail" to the 2nd order (I_{tail}/I_2) is 0.0173/0.0081 (about 2.135). We can also obtain the value of I_{tail}/I_2 according to the horizontal diffraction distribution of Fig. 10(a), which is equal to 0.639/0.333 (about 1.919). This shows the above simulation based on the screen function is effective.

Second, we try to explore the relationship between the fabrication performance and the diffraction pattern. For pure sinusoidal gratings, the 2nd-order diffraction should not appear,

Optics EXPRESS

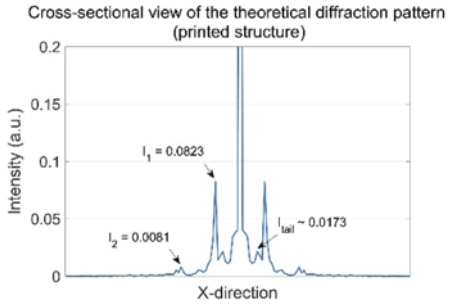

Fig. 11. The cross-sectional view of the theoretical diffraction pattern of the fabricated microstructure. I_1 and I_2 are the intensity peak values corresponding to the 1st order and the 2nd order, I_{tail} is the average intensity value of the "tail" between the zero order and 1st order.

while for pure binary gratings, the intensity of the 1st and 2nd-order should be much larger (over 60% for I_1). Obviously, the profile of the fabricated microstructures can be fitted by the higher-order Fourier functions. And theoretically, for a given light intensity distribution of diffraction orders, the higher the Fourier terms can be fitted, the better the fabrication performance is, that is, the higher the contrast of the microstructure is.

By fitting the periodic step function shown in Fig. 8 (c), we obtain that each diffraction order is introduced by a Fourier term of the corresponding order, as shown in Fig. 12. We find that a very small peak appears next to the 1st-order diffraction in Fig. 12(b).The small peak is the true 2nd-order diffraction according to the grating equation, and the peak with an intensity of 0.0164 in Fig. 12(d) is actually the 3rd-order diffraction because the 2nd order is missing due to interference. In applications of fiber-tip beam splitter, higher light intensity is expected to enter non-zero diffraction orders. Hence, the profile of fabricated microstructures should be closer to the standard periodic step functions. By measuring the distance from "top" to "bottom" of the fitted Fourier function, we obtain that the steepness angle θ_2 of the fitted 3rd-order Fourier function is about 15.03°. The steepness of the fabricated structure will be a little bit less than that. In future research, optimizing the contrast of fabricated microstructures will greatly contribute to the diffraction performance as expected.

The experimental results illustrate that it is effective to fabricate functional optical microstructures directly on the SMF end faces by the DMD-based lithography method we proposed. For the method previously reported by *Kim et al.* [35], a section of CLF with a length of less than 1 mm was fusion-spliced with an SMF, which was aimed to expand the output beam. By the fusion-splicing method, the effective area of the fiber core was enlarged to a certain extent. However, the change of some optical parameters such as NA will cause trouble for the application of this kind of fiber. In this study, the method we proposed is not limited to the hybrid optical fiber comprising an SMF with a CLF. Hence, this method possesses higher adaptability and flexibility.

Although the fabrication resolution of 0.405 μm can be achieved, there are still certain limitations caused by the tiny effective area of the SMF end face. One optimistic case is that, when fabricating the linear gratings or the Ronchi gratings, the facet of the SMF fiber core can be covered with about 11 periods of the microstructures. However, when fabricating the complex microstructures which include more features in each period, such as Dammann gratings, only 1 period can be fabricated on the facet of the SMF fiber core. Therefore, while maintaining the advantage of low cost, further research on this work should be concentrated on continuously improving the fabrication resolution to the deep sub-micron scale.

Optics EXPRESS

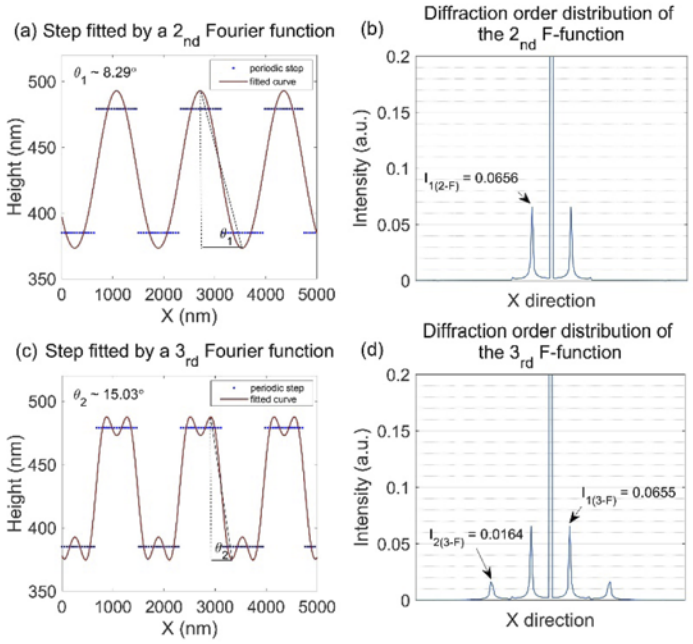

Fig. 12. Fitting the fitted periodic step function by 2nd-order and 3rd-order Fourier functions respectively. In (a) and (c), the X and Y axis are not proportional and the values of the angles are labeled in the upper left corner.

5. Conclusions

In this study, an effective microfabrication method based on DMD maskless lithography is proposed, which enables the convenient fabrication of sub-micron scale functional optical microstructures on the optical fiber end faces. Besides, a specialized photoresist spin-coating device for the optical fiber end faces is designed. The experimental results of fabricating microstructures show that the DMD based lithography system we proposed can provide a high fabrication resolution of 0.405 μm within an exposure area of 209.92 μm 157.44 μm. Furthermore, we observe the optical diffraction modulation effects of the functional optical microstructures fabricated on the SMF end faces by coupling a visible light beam into another side of the optical fiber, hence once again verifying the validity and application value of this method. Due to its advantages of low cost, high efficiency, and relatively high resolution, this fabrication method provides a new pathway for the rapid fabrication of optical fiber devices.

Funding. National Natural Science Foundation of China (61464008, 61704070); Natural Science Foundation of Jiangxi Province (20202BAB202012).

Disclosures. The authors declare no conflicts of interest.

Data availability. Data underlying the results presented in this paper are not publicly available at this time but may be obtained from the authors upon reasonable request.

Optics EXPRESS

References

1. C.-Y. Chang, Y. Y. Hu, C.-Y. Lin, C.-H. Lin, H.-Y. Chang, S.-F. Tsai, T.-W. Lin, and S.-J. Chen, "Fast volumetric imaging with patterned illumination via digital micro-mirror device-based temporal focusing multiphoton microscopy," Biomed. Opt. Express **7**(5), 1727–1736 (2016).
2. W. Chen, W. Han, D. C. Abeysinghe, R. L. Nelson, and Q. Zhan, "Generating cylindrical vector beams with subwavelength concentric metallic gratings fabricated on optical fibers," J. Opt. **13**(1), 015003 (2011).
3. G.-h. Shao, S.-c. Yan, W. Luo, G.-W. Lu, and Y.-q. Lu, "Orbital angular momentum (OAM) conversion and multicasting using N-core supermode fiber," Sci. Rep. **7**(1), 1062 (2017).
4. T. Gissibl, S. Thiele, A. Herkommer, and H. Giessen, "Two-photon direct laser writing of ultracompact multi-lens objectives," Nature Photon **10**(8), 554–560 (2016).
5. H. Ghafoori-shiraz and T. Asano, "Microlens for coupling a semiconductor laser to a single-mode fiber," Opt. Lett. **11**(8), 537–539 (1986).
6. L. G. Cohen and M. V. Schneider, "Microlenses for Coupling Junction Lasers to Optical Fibers," Appl. Opt. **13**(1), 89–94 (1974).
7. S. Deepa, B. R. B.S.. , and P. Senthilkumaran, "Helicity dependent diffraction by angular momentum transfer," Sci. Rep. **9**(1), 12491 (2019).
8. X. Zhao, N. Zhao, Y. Shi, H. Xin, and B. Li, "Optical Fiber Tweezers: A Versatile Tool for Optical Trapping and Manipulation," Micromachines **11**(2), 114 (2020).
9. G. Anastasiadi, M. Leonard, L. Paterson, and W. N. Macpherson, "Fabrication and characterization of machined multi-core fiber tweezers for single cell manipulation," Opt. Express **26**(3), 3557–3567 (2018).
10. R. S. Rodrigues Ribeiro, P. Dahal, A. Guerreiro, P. A. S. Jorge, and J. Viegas, "Fabrication of Fresnel plates on optical fibres by FIB milling for optical trapping, manipulation and detection of single cells," Sci. Rep. **7**(1), 4485 (2017).
11. C. Liberale, P. Minzioni, F. Bragheri, F. De Angelis, E. Di Fabrizio, and I. Cristiani, "Miniaturized all-fibre probe for three-dimensional optical trapping and manipulation," Nature Photon **1**(12), 723–727 (2007).
12. G. Kostovski, P. R. Stoddart, and A. Mitchell, "The optical fiber tip: an inherently light-coupled microscopic platform for micro- and nanotechnologies," Adv. Mater. **26**(23), 3798–3820 (2014).
13. R. S. Rodrigues Ribeiro, P. Dahal, A. Guerreiro, P. Jorge, and J. Viegas, "Optical fibers as beam shapers: from Gaussian beams to optical vortices," Opt. Lett. **41**(10), 2137–2140 (2016).
14. S. Scheerlinck, D. Taillaert, D. Van Thourhout, and R. Baets, "Flexible metal grating based optical fiber probe for photonic integrated circuits," Appli. Phys. Lett. **92**(3), 031104 (2008).
15. S. Y. Ryu, H. Y. Choi, J. Na, W. J. Choi, and B. H. Lee, "Lensed fiber probes designed as an alternative to bulk probes in optical coherence tomography," Appl. Opt. **47**(10), 1510–1516 (2008).
16. T. Gissibl, S. Thiele, A. Herkommer, and H. Giessen, "Sub-micrometre accurate free-form optics by three-dimensional printing on single-mode fibres," Nat. Commun. **7**(1), 11763 (2016).
17. S. Schmidt, S. Thiele, A. Toulouse, C. Bösel, T. Tiess, A. Herkommer, H. Gross, and H. Giessen, "Tailored micro-optical freeform holograms for integrated complex beam shaping," Optica **7**(10), 1279–1286 (2020).
18. S. H. Lee, S. E. Seo, K. H. Kim, J. Lee, C. S. Park, B.-H. Jun, S. J. Park, and O. S. Kwon, "Single photomask lithography for shape modulation of micropatterns," J. Ind. Eng. Chem. **84**, 196–201 (2020).
19. A. Koshelev, G. Calafiore, C. Pina-Hernandez, F. I. Allen, S. Dhuey, S. Sassolini, E. Wong, P. Lum, K. Munechika, and S. Cabrini, "High refractive index Fresnel lens on a fiber fabricated by nanoimprint lithography for immersion applications," Opt. Lett. **41**(15), 3423–3426 (2016).
20. M. A. Verschuuren, M. Megens, Y. Ni, H. van Sprang, and A. Polman, "Large area nanoimprint by substrate conformal imprint lithography (SCIL)," Adv. Opt. Technol. **6**(3-4), 243–264 (2017).
21. M. A. Verschuuren, M. W. Knight, M. Megens, and A. Polman, "Nanoscale spatial limitations of large-area substrate conformal imprint lithography," Nanotechnology **30**(34), 345301 (2019).
22. Y. Lin, Y. Zou, Y. Mo, J. Guo, and R. G. Lindquist, "E-beam patterned gold nanodot arrays on optical fiber tips for localized surface plasmon resonance biochemical sensing," Sensors **10**(10), 9397–9406 (2010).
23. N. Wang, M. Zeisberger, U. Hübner, and M. A. Schmidt, "Nanotrimer enhanced optical fiber tips implemented by electron beam lithography," Opt. Mater. Express **8**(8), 2246–2255 (2018).
24. S. Feng, S. Darmawi, T. Henning, P. J. Klar, and X. Zhang, "A miniaturized sensor consisting of concentric metallic nanorings on the end facet of an optical fiber," Small **8**(12), 1937–1944 (2012).
25. R. Janeiro, R. Flores, P. Dahal, and J. Viegas, "Fabrication of a phase photon sieve on an optical fiber tip by focused ion beam nanomachining for improved fiber to silicon photonics waveguide light coupling," Opt. Express **24**(11), 11611–11625 (2016).
26. J. Han, M. Sparkes, and W. O'Neill, "Controlling the optical fiber output beam profile by focused ion beam machining of a phase hologram on fiber tip," Appl. Opt. **54**(4), 890–894 (2015).
27. T. Gissibl, M. Schmid, and H. Giessen, "Spatial beam intensity shaping using phase masks on single-mode optical fibers fabricated by femtosecond direct laser writing," Optica **3**(4), 448–451 (2016).
28. K. Weber, F. Hutt, S. Thiele, T. Gissibl, A. Herkommer, and H. Giessen, "Single mode fiber based delivery of OAM light by 3D direct laser writing," Opt. Express **25**(17), 19672–19679 (2017).
29. C. Zhang, Z. Jiang, S. Fu, M. Tang, W. Tong, and D. Liu, "Femtosecond laser enabled selective micro-holes drilling on the multicore-fiber facet for displacement sensor application," Opt. Express **27**(8), 10777–10786 (2019).

Optics EXPRESS

30. C. Liberale, G. Cojoc, P. Candeloro, G. Das, F. Gentile, F. D. Angelis, and E. D. Fabrizio, "Micro-Optics Fabrication on Top of Optical Fibers Using Two-Photon Lithography," IEEE Photonics Technol. Lett. **22**(7), 474–476 (2010).
31. M. Malinauskas, A. Žukauskas, V. Purlys, K. Belazaras, A. Momot, D. Paipulas, R. Gadonas, A. Piskarskas, H. Gilbergs, A. Gaidukevičiūtė, I. Sakellari, M. Farsari, and S. Juodkazis, "Femtosecond laser polymerization of hybrid/integrated micro-optical elements and their characterization," J. Opt. **12**(12), 124010 (2010).
32. P. Somers, Z. Liang, J. E. Johnson, B. W. Boudouris, L. Pan, and X. Xu, "Rapid, continuous projection multi-photon 3D printing enabled by spatiotemporal focusing of femtosecond pulses," Light Sci Appl **10**(1), 199 (2021).
33. M. Vasileia, M. Farsari, and S. Pissadakis, "A Fiber Optic Fabry–Perot Cavity Sensor for the Probing of Oily Samples," Fibers **5**(1), 1 (2017).
34. E. Kabouraki, V. Melissinaki, A. Yadav, A. Melninkaitis, K. Tourlouki, T. Tachtsidis, N. Kehagias, G. D. Barmparis, D. G. Papazoglou, E. Rafailov, and M. Farsari, "High laser induced damage threshold photoresists for nano-imprint and 3D multi-photon lithography," Nanophotonics **10**(14), 3759–3768 (2021).
35. J. B. Kim and K. H. Jeong, "Batch fabrication of functional optical elements on a fiber facet using DMD based maskless lithography," Opt. Express **25**(14), 16854–16859 (2017).
36. Q. Zheng, J. Zhou, Q. Chen, L. Lei, K. Wen, and Y. Hu, "Rapid Prototyping of a Dammann Grating in DMD-Based Maskless Lithography," IEEE Photonics J. **11**, 1–10 (2019).
37. X. Ma, Y. Kato, F. van Kempen, Y. Hirai, T. Tsuchiya, F. van Keulen, and O. Tabata, "Experimental Study of Numerical Optimization for 3-D Microstructuring Using DMD-Based Grayscale Lithography," J. Microelectromech. Syst. **24**(6), 1856–1867 (2015).
38. N. Luo, G. Xu, Z. Zhang, and W. Zhang, "Reduction of buried microstructure diffraction in fabricating curved microstructure by multiple exposure method," Opt. Express **26**(24), 31085–31093 (2018).
39. J. Liu, J. Liu, Q. Deng, J. Feng, S. Zhou, and S. Hu, "Intensity modulation based optical proximity optimization for the maskless lithography," Opt. Express **28**(1), 548–557 (2020).
40. R. Chen, H. Liu, H. Zhang, W. Zhang, J. Xu, W. Xu, and J. Li, "Edge smoothness enhancement in DMD scanning lithography system based on a wobulation technique," Opt. Express **25**(18), 21958–21968 (2017).
41. Z. Zhang, Y. Gao, N. Luo, K. Zhong, and Z. Liu, "Multi-direction digital moving mask method for fabricating continuous microstructures," Opt. Appl. **45**(1), 79–88 (2015).
42. C. Zhou and L. Liu, "Numerical study of Dammann array illuminators," Appl. Opt. **34**(26), 5961–5969 (1995).